Electronic structure and the valence state of Yb$_2$Pd$_2$Sn and YbPd$_2$Sn studied by photoelectron and resonant x-ray emission spectroscopies

Hithoshi Yamaoka,[1] Patrik Thunström,[2] Naohito Tsujii,[3] Ignace Jarrige,[4,*] Kenya Shimada,[5] Masashi Arita,[5] Hideaki Iwasawa,[5] Hirokazu Hayashi,[5] Jian Jiang,[5] Hirofumi Namatame,[5] Masaki Taniguchi,[5] Nozomu Hiraoka,[6] Hirofumi Ishii,[6] Ku-Ding Tsuei,[6] Mauro Giovannini,[7] and Ernst Bauer[8]

[1]*Harima Institute, RIKEN (The Institute of Physical and Chemical Research), Sayo, Hyogo 679-5148, Japan*
[2]*Department of Physics and Mathematical Science, Uppsala University, P.O. Box 530, SE-75121, Uppsala, Sweden*
[3]*Quantum Beam Center, National Institute for Materials Science, 1-2-1 Sengen, Tsukuba 305-0047, Japan*
[4]*Japan Atomic Energy Agency, SPring-8, Sayo, Hyogo 679-5148, Japan*
[5]*Hiroshima Synchrotron Radiation Center, Hiroshima University, Higashi-Hiroshima, Hiroshima 739-0046, Japan*
[6]*National Synchrotron Radiation Research Center, Hsinchu 30076, Taiwan*
[7]*CNR-SPIN, Dipartimento di Chimica e Chimica Industriale, University of Genova, Italy*
[8]*Institute of Solid State Physics, Vienna University of Technology, Wien 1040, Austria*
(Received 6 June 2012; revised manuscript received 30 July 2012; published 24 August 2012)

We have examined the electronic structure of the heavy fermion Yb$_2$Pd$_2$Sn in comparison with the superconductor YbPd$_2$Sn by means of high-resolution photoelectron spectroscopy (PES) and resonant x-ray emission spectroscopy (RXES). The PES data are interpreted in light of the density of states calculated within the local density approximation plus the dynamical mean-field theory. Our analysis of the RXES data shows that the valence of Yb in Yb$_2$Pd$_2$Sn is weakly fluctuating, indicating weak but finite c-f hybridization, and decreases slightly with temperature. In contrast, the Yb valence in YbPd$_2$Sn is nearly $3+$ and does not show any temperature dependence, suggesting that the Yb $4f$ electrons are localized and the superconductivity is due to the Pd conduction electrons. The constant initial state spectra at the Yb $4d$-$4f$ resonance for Yb$_2$Pd$_2$Sn clearly show resonant behavior for Yb^{3+} and antiresonance for Yb^{2+}, indicating that the Yb^{3+} and Yb^{2+} states are intimately correlated.

I. INTRODUCTION

In Yb-based intermetallic compounds, the fluctuation between magnetic Yb^{3+} ($4f^{13}$) and nonmagnetic Yb^{2+} ($4f^{14}$) can provide an additional degree of freedom on pressure- or temperature-driven ground states.[1,2] Such physical properties are closely related to the interaction between the $4f$ and the conduction electrons, which leads to either an ordering of the local moments through the Ruderman-Kittel-Kasuya-Yoshida (RKKY) interaction or a screening of the local moments due to the Kondo effect.[3–5] Ternary compounds R_2T_2M (R: rare earth, T: transition metal, M: Cd, In, Sn, and Pb) are attracting much attention because of their rich variety of exotic physical phenomena, which are seemingly linked to the competition between the RKKY and the Kondo interactions.[6–14]

Among them, Yb$_2$Pd$_2$Sn was recently found to exhibit two pressure-driven quantum critical points (QCPs).[11,15,16] A pressure-induced magnetic instability occurs at 1 GPa (the first QCP), whereas, further pressure increases result in a domelike magnetic phase, which vanishes above 4 GPa (the second QCP). The crystal structure is tetragonal with two types of layers alternatively stacking along the c axis. The first layer containing R atoms is arranged in a triangular geometry, and the second layer includes T and M atoms. Thus, a scenario based on the geometrical frustration forming the Shastry-Sutherland lattice[14] has been proposed to explain the occurrence of the two QCPs beyond the conventional frame of the competition between the RKKY and the Kondo effect.[17] Another scenario based on the single impurity Anderson model (SIAM) accounting for a pressure-driven suppression of valence fluctuation was also suggested.[15,18]

The temperature dependence of some of the physical properties of Yb$_2$Pd$_2$Sn is also anomalous. Temperature dependences of both electric resistivity and specific heat pointed to a non-Fermi-liquid ground state.[15] The temperature dependence of the resistivity shows two maxima around 200 and 11 K, which are thought to arise from a combined interplay among the RKKY interaction, the Kondo effect, and the crystal electric field (CEF) splitting.[11] The magnetic susceptibility shows a broad peak at low temperatures.[17] The electronic specific coefficient is 560 mJ mol^{-1} K^{-2} (Refs. 11 and 19), indicating heavy fermion behavior. No magnetic order down to 0.1 K has been reported,[11] although the Yb valence was estimated to be close to the $3+$ state from the x-ray absorption measurement at the Yb L_3 edge.[11,15]

Although the crystal structure and the peculiar transport properties of Yb$_2$Pd$_2$Sn have already been thoroughly investigated, no measurement of its electronic structure has been reported yet. In this paper, we report high-resolution photoelectron spectroscopy (PES) and resonant x-ray emission spectroscopy (RXES) measurements of Yb$_2$Pd$_2$Sn at ambient pressure and as a function of temperature in an effort to address the abnormal temperature and pressure dependences of its physical properties. For comparison, we also report a measurement of the electronic structure of the superconductor YbPd$_2$Sn, which we use here as a reference for a purely trivalent Yb ternary system.[20,21] The temperature dependence of the valence-band spectra near the Fermi edge is measured using both ultraviolet (UV) and soft x-ray (SX) photon energies. The temperature dependence of the Yb valence is derived using a combination of RXES and x-ray absorption spectroscopy
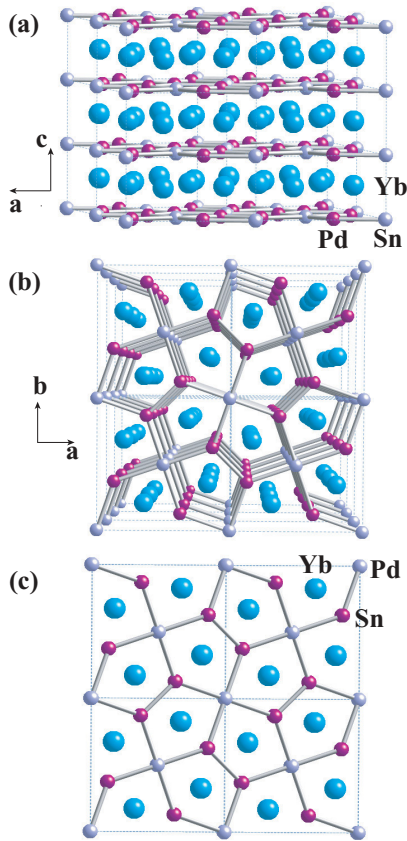
FIG. 1. (Color online) Schematic of the crystal structure of Yb_2Pd_2Sn: (a) a perspective view of the *ac* plane, (b) a perspective view of the *ab* plane, and (c) a projection on the *ab* plane.

in the partial fluorescence mode (PFY-XAS).[2,22–24] Resonant PES in both UV and SX energy regions is also performed. We compare the multiplet structure of the photoelectron spectra with the density of states (DOS) calculated using a combination of density-functional theory in the local density approximation (LDA), dynamical mean-field theory (DMFT), and the Hubbard-I approximation.[25–29]

II. EXPERIMENTS AND CALCULATIONS

A. Experiments and analyses

Polycrystalline samples of Yb_2Pd_2Sn and $YbPd_2Sn$ were prepared in a closed tantalum tube with an Ar atmosphere at $1300\,°C$ for 1.5 h by a high-frequency induction furnace and then were annealed at $980\,°C$ for 10 days. Yb_2Pd_2Sn has the Mo_2FeB_2-type tetragonal crystal structure (space group $P4/mbm$) with lattice constants of $a = 0.7573$ and $c = 0.3638$ nm as shown in Fig. 1. $YbPd_2Sn$ crystallizes in a Heusler-type cubic-crystal structure (space group $Fm\bar{3}m$, $a = 0.6635$ nm) with a superconducting transition temperature of $T_{SC} = 2.3$ K and a Néel temperature of $T_N = 0.22$ K. The electronic specific coefficient is $6\ mJ\,K^{-2}\,mol^{-1}$.[20,21] The magnetic susceptibility was measured with a superconducting quantum interference device magnetometer at an applied field of 1000 Oe. SX and UV PES measurements were performed at the undulator beamlines BL-1 and BL-9A at the Hiroshima Synchrotron Radiation Center (HiSOR), equipped with high-

resolution hemispherical electron-energy analyzers (R4000, VG-SCIENTA).[30,31] In the UV PES, the energy resolution (ΔE) was set to be less than about 10 meV at $h\nu = 11$ eV and 9 K under the vacuum pressure below 2×10^{-9} Pa, where $h\nu$ is the incident photon energy. In the SX PES, ΔE was set to 40–50 meV around $h\nu = 182$ eV and 8 K under the vacuum pressure below 10^{-8} Pa. The Fermi edge of Au, evaporated on the sample holders, was used to calibrate the binding energy. All samples were fractured in vacuum just before the measurements. The energy resolution and the Fermi level are determined with a fit of the Fermi edge of Au using a convolution of a Gaussian and a Fermi-Dirac function.

PFY-XAS and RXES measurements were performed at the Taiwan beamline BL12XU, SPring-8.[2,22–24] The undulator beam was monochromatized by a pair of cryogenically cooled Si(111) crystals and was focused to a size of 30 (horizontal) × 40 (vertical) μm^2 at the sample position using toroidal and Kirkpatrick-Baez mirrors. The incident photon flux was estimated to be about 10^{13} photons/s at 8.94 keV from the measurement by using a pin diode (type S3590-09). A Johann-type spectrometer equipped with a spherically bent Si(620) crystal (radius of ∼1 m) was used to analyze the Yb $L\alpha_1$ ($3d_{5/2} \rightarrow 2p_{3/2}$) and Raman emissions with a solid-state detector (XFlash 1001, type 1201). The overall energy resolution was estimated to be about 1 eV around the emitted photon energy of 7400 eV from the elastic scattering. The intensities of all spectra are normalized by the incident beam intensity monitored just before the target.

B. Calculations

A fully charged self-consistent LDA + DMFT calculation[32,33] was performed, using the full-potential linear muffin-tin orbital code RSPt (Ref. 34) and the DMFT implementation presented in Refs. 25, 35, and 36. The strongly correlated Yb $4f$ states were treated with the Hubbard-I approximation.[37,38] The local Coulomb interaction among the Yb $4f$ electrons was parametrized in terms of the Slater parameters F^0, F^2, F^4, and F^6. The parameters F^2, F^4, and F^6 were calculated at the beginning of each new LDA iteration through a radial integration of the unscreened local Coulomb interaction and then were scaled by 0.92, 0.97, and 1.00, respectively. These scaling constants account for the screening by the non-f electrons and are roughly material independent.[29] The final fully self-consistent values are $F^2 = 14.2$, $F^4 = 9.3$, and $F^6 = 6.9$ eV. The Hubbard U parameter F^0 cannot be calculated in the same way as it is too strongly screened. Instead, it was set to the constant value of 7.9 eV. The **k** points used in the calculations of Yb_2Pd_2Sn and $YbPd_2Sn$ were distributed in a $8 \times 8 \times 12$ and $12 \times 12 \times 12$ Monkhorst-Pack grid, respectively. The Brillouin-zone integration was carried out using Fermi smearing with $T = 273$ K.

III. RESULTS AND DISCUSSION

A. Magnetic susceptibility

The temperature dependence of the magnetic susceptibility χ of Yb_2Pd_2Sn is shown in Fig. 2. χ decreases above $T \sim 10$ K. We fit the $1/\chi$ curve with the formula $1/\chi = (T - \Theta_p)/C$ at $T \geqslant 100$ K, where Θ_p and C are the Weiss

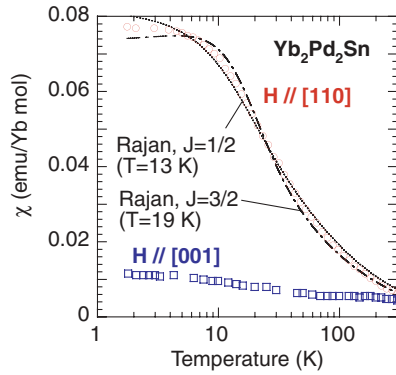FIG. 2. (Color online) Magnetic susceptibility as a function of temperature for Yb_2Pd_2Sn. Susceptibilities along [110] and [001] are shown as open circles and open squares, respectively. Fit curves based on the single impurity Anderson model[39] are also shown.

temperature and the Curie constant, respectively. We obtain $C = 2.00$ and $\Theta_p = -12.8$ K. The negative Weiss temperature suggests valence fluctuations of Yb. The Curie constant is written as $C = N_A\mu_{eff}^2/3k_B$, where μ_{eff}, N_A, and k_B are the effective magnetic moment, the Avogadro number, and the Boltzmann constant, respectively. In the valence-fluctuating Yb systems, the effective magnetic moment can be used as a measure of the degree of valence admixture since the Yb^{3+} ($4f^{13}$, $J = 7/2$) ion has a magnetic moment, whereas, Yb^{2+} ($4f^{14}$, $J = 0$) is nonmagnetic. μ_{eff} is estimated to be $3.99\mu_B$, which is smaller than $4.54\mu_B$ for the Yb^{3+} ion calculated with the formula according to Hund's rule $\mu_{eff} = g\sqrt{J(J+1)}\mu_B$, where g is the Landé g factor. It indicates that Yb is nearly a trivalent ground state with a small fraction of a divalent component.

According to the Bethe ansatz solution of the Coqblin-Schrieffer model based on the SIAM, the physical properties of a Kondo material are well scaled by a single energy parameter, the characteristic temperature T_0.[39] We estimate T_0 by using Rajan's numerical results as shown in Fig. 2. By taking into account the lift of the degeneracy due to the CEF of 250 K (first excited state),[17] we obtain $T_0 = 13$ and 19 K with the fits of Rajan's curve for the angular momenta of $J = 1/2$ and $3/2$, respectively. These values are comparable to $T_K = 15$ K estimated from fit to the specific heat.[11]

B. LDA + DMFT calculations

Figure 3 shows the calculations of the total [Figs. 3(a) and 3(c)] and the $4f$ [Figs. 3(b) and 3(d)] DOS of Yb_2Pd_2Sn and $YbPd_2Sn$, respectively. A linewidth of 0.01 Ry (0.136 eV) was used for the comparison with the experimental results. In Fig. 3(b), the structures lying within $E_b = 0$–4 eV and $E_b = 4$–12 eV, respectively, correspond to Yb^{2+} and Yb^{3+}. The calculations of the Yb $4f$ DOS are in good agreement with the experimental spectra for both Yb_2Pd_2Sn at $h\nu = 170$ and 182 eV and $YbPd_2Sn$ at $h\nu = 182$ eV, respectively, as shown in Figs. 3(b) and 3(d), except for the broad surface-derived Yb^{2+} peaks on the high-binding energy side of the bulk-derived ones in the experimental spectra. For the resonant effect, it will be discussed below. We note that the Yb $4f$ photoionization cross section is large in this incident
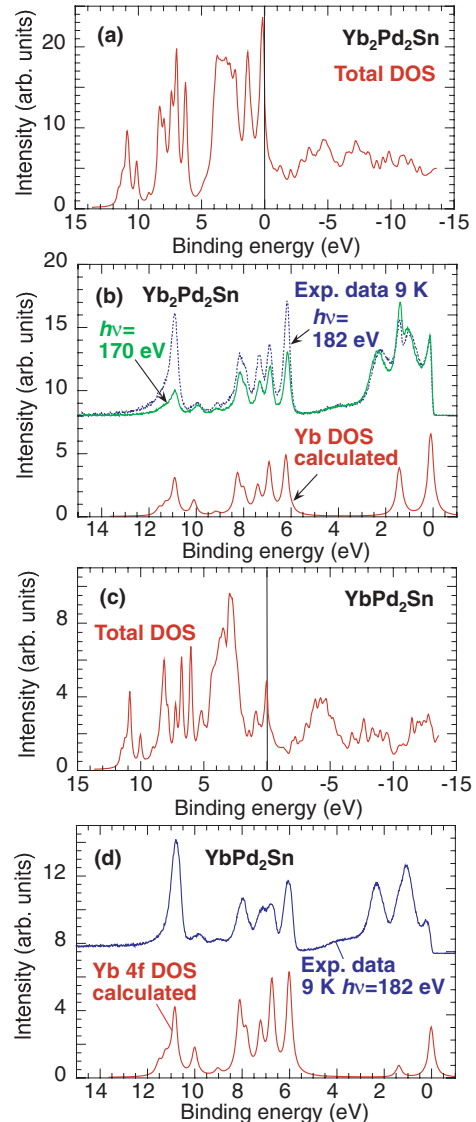

FIG. 3. (Color online) Result of the DOS calculated with LDA + DMFT with a spectral line broadening of 0.01 Ry (0.136 eV) for Yb_2Pd_2Sn and $YbPd_2Sn$. (a) Total DOS for Yb_2Pd_2Sn. (b) Yb $4f$ DOS for Yb_2Pd_2Sn with measured spectra at $h\nu = 182$ eV (on-resonance, dotted-line) and 170 eV (off-resonance, solid-line) at 9 K. Note that the background is subtracted from the experimental data. The same data are also used in Fig. 6 and are partly used in Fig. 7. (c) Total DOS for $YbPd_2Sn$. (d) Yb $4f$ DOS for $YbPd_2Sn$ with measured spectra at $h\nu = 182$ eV (on-resonance) at 9 K.

energy range, therefore, the obtained experimental spectra are suitable for comparison with the calculated Yb $4f$ DOS. It is noteworthy that both the PES spectra and the calculated Yb $4f$ DOS are very similar for both $YbPd_2Sn$ and Yb_2Pd_2Sn despite their different crystal structures.

In Yb_2Pd_2Sn, the inelastic mean-free path of the photoelectrons is estimated to be on the order of 0.6 nm at $h\nu = 182$ eV,[29,40] which is comparable to the lattice constants of $a = 0.7573$ and $c = 0.3638$ nm. The inelastic electron mean-free path of $YbPd_2Sn$ at $h\nu = 182$ eV is estimated to be on the order of 0.75 nm, which is comparable to the value for Yb_2Pd_2Sn. Thus, the intensities of the surface Yb^{2+}
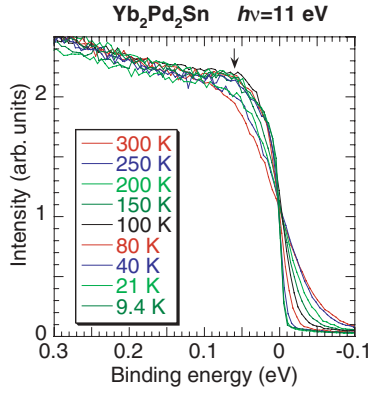
FIG. 4. (Color online) Valence-band spectra near the Fermi edge as a function of temperature for Yb_2Pd_2Sn at $h\nu = 11$ eV.

component are also comparable as shown in Figs. 3(b) and 3(d), and we observe the surface components in $YbPd_2Sn$ as well as in Yb_2Pd_2Sn. At the surface, Yb is less coordinated, the cohesive energy of the surface Yb atoms is smaller than that of the bulk Yb atoms, and the surface Yb atoms tend to be divalent.

C. Temperature dependence

We measured the valence-band spectrum of Yb_2Pd_2Sn at $h\nu = 11$ eV as a function of temperature as shown in Fig. 4. There is a finite DOS at the Fermi level from room temperature to low temperatures. At $h\nu = 11$ eV, the photoionization cross section of Yb $4f$ is 1 order smaller than those of Pd $4d$ and Sn $5p$ (Ref. [41]) so that the DOS near the Fermi level mainly consists of the Pd $4d$ and Sn $5p$ DOS. We should note, however, that we can identify a spectral feature at $E_b \sim 0.06$ eV where the Yb $4f_{7/2}$ state exists in the Yb $4d$-$4f$ on-resonance spectra as shown below.

In order to measure the temperature dependence of the Yb valence, we employed the bulk-sensitive RXES method. Figures 5(a) and 5(b), respectively, show the temperature dependence of the Yb-L_3 PFY-XAS spectrum and of the Yb $2p_{3/2}$-$3d_{5/2}$ RXES spectra measured at the Yb^{2+} resonance at $h\nu = 8938$ eV for Yb_2Pd_2Sn. The RXES spectra are shown as a function of the energy transfer, which is defined as the difference between the incident photon and the emitted photon energies. These spectra clearly show that Yb in Yb_2Pd_2Sn is weakly valence fluctuating, consisting mainly of Yb^{3+} with a small faction of Yb^{2+}. The values of the Yb valence derived from the fit of the PFY-XAS spectra for Yb_2Pd_2Sn are shown in Fig. 5(c) along with the intensity ratio of Yb^{2+} to Yb^{3+} estimated from the fit of the RXES spectra at $h\nu = 8938$ eV.[2,23,24] Our estimate of the Yb valence at 20 K is in good agreement with a previous paper (Yb valence of 2.91 ± 0.03) that used conventional XAS.[11] It is noted that higher valences in hard x-ray bulk-sensitive XAS studies are often obtained compared with the PES estimations as described below.[42] This likely reflects the difficulty in properly disentangling the surface and bulk components from each other in the PES valence-band spectra.

In Fig. 5(d), the temperature dependence of the Yb valence and of the intensity ratio of Yb^{2+} to Yb^{3+} is shown for $YbPd_2Sn$. We find the Yb valence in $YbPd_2Sn$ to be
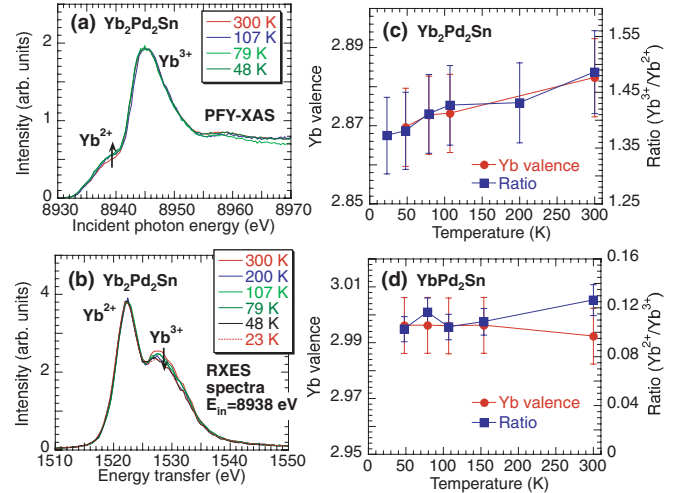

FIG. 5. (Color online) (a) PFY-XAS spectra for Yb_2Pd_2Sn as a function of temperature. (b) RXES spectra for Yb_2Pd_2Sn at the incident photon energy of 8938 eV as a function of temperature. (c) Yb valence estimated from the PFY-XAS spectra for Yb_2Pd_2Sn (closed circle) with the intensity ratio of Yb^{2+} to Yb^{3+} (closed square) as a function of temperature. (d) Yb valence for $YbPd_2Sn$ (closed circle) with the intensity ratio of Yb^{2+} to Yb^{3+} (closed square) as a function of temperature.

temperature independent within the error bars. Furthermore, the Yb valence in $YbPd_2Sn$ is nearly $3+$, suggesting the localized Yb $4f$ electrons without c-f hybridization. Thus, the superconductivity is due to the Pd conduction electrons. Usually, in Kondo Yb materials, the valence starts to decrease rapidly below T_K.[23] However, our results show a very small and monotonous decrease in the valence with temperature for Yb_2Pd_2Sn, which can be explained by the fact that the temperature range of the measurement is higher than T_K (15 K).[23] Another important parameter that one needs to take into account in order to understand the temperature dependence of the valence, in addition to the Kondo temperature, is the CEF effect.[43] The CEF in Yb_2Pd_2Sn is about 250 K (Ref. [17]), which is much larger than the Kondo temperature and which should, therefore, result in a weak temperature dependence of the valence. The temperature dependence of the valence of Yb_2Pd_2Sn shows a normal Kondo-like behavior, which can be understood within the SIAM. In $YbPd_2Sn$, the Yb bulk valence does not show any temperature dependence, and the mean-Yb valence is nearly trivalent, suggesting a much weaker c-f hybridization compared to Yb_2Pd_2Sn.

D. Resonant PES

Figure 6(a) shows the valence-band spectra measured at $h\nu = 182$ eV for Yb_2Pd_2Sn, where the Yb $4d$-$4f$ resonance occurs. The Yb $4f$ states can be observed owing to the increase in the $4f$ photoionization cross section in this energy region,[41] whereas, no $4f$ spectral feature was observed in the valence-band spectra at $h\nu = 11$ eV. In the valence-band spectra, the Yb^{2+} surface components can be separated from the bulk ones experimentally because of the difference in the binding energies. We find that the energy shift between the
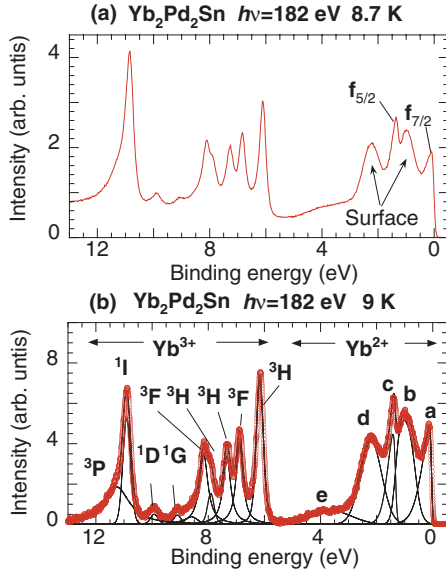
FIG. 6. (Color online) (a) Resonant valence-band spectra for Yb$_2$Pd$_2$Sn at $h\nu = 182$ eV and 9 K. (b) Example of the fit for the spectrum of Yb$_2$Pd$_2$Sn at 9 K and $h\nu = 182$ eV after extracting the background.

surface and the bulk Yb^{2+} components is about 0.83 eV, which is larger than the theoretical prediction.[44] Figure 6(b) shows an example of the fit after subtracting the background for Yb$_2$Pd$_2$Sn at $h\nu = 182$ eV and 9 K. Based on the calculations in Fig. 3(b), peaks a and c in Yb^{2+} are assigned to the bulk components of $4f_{7/2}$ and $4f_{5/2}$, and peaks b and d are assigned to their surface contributions. Peaks for Yb^{3+} are assigned, too, as shown in Fig. 6(b). Peak e is the contribution from Pd and Sn DOS.

The measurements of the resonant valence-band spectra as a function of the incident photon energy are performed across the Yb $4d$ absorption edge for Yb$_2$Pd$_2$Sn at 8 K as shown in Fig. 7(a). Figure 7(b) shows constant initial state (CIS) spectra for each component in Fig. 6(b) as a function of the incident photon energies. Yb^{3+} has a hole in the $4f$ states ($4f^{13}$), and thus, a $4d$-$4f$ resonant enhancement of the intensity occurs. A Fano profile is observed for Yb^{3+} as shown in Fig. 7(b). On the other hand, the intensity of the CIS spectra for both bulk and surface Yb^{2+} ($4f^{14}$) components resonantly decreases. The electron emissions from direct photoionization processes and super-Coster-Kronig-Auger decay processes, respectively, are written as

$$h\nu + 4d^{10}4f^{13} \rightarrow 4d^{9}4f^{14} \rightarrow 4d^{10}4f^{12}\epsilon l + e_k,$$
$$h\nu + 4d^{10}4f^{13} \rightarrow 4d^{10}4f^{12}\epsilon l + e_k,$$

where e_k is the emitted electrons.[29,45] They have the same initial and final states, and thus, the Fano profile can be observed if the interaction occurs between the discrete state ($4d^{9}4f^{14}$) and the continuum state ($4d^{10}4f^{12}\epsilon l + e_k$). The CIS spectra are well fitted with the Fano profile $I = I_0 + I_1(q + E)^2/(1 + E^2)$ [$E = (h\nu - E_0)/\Gamma$] as shown in Fig. 7(b) with solid lines, where E_0, Γ, and q are resonant photon energy, half-width of the line, and asymmetry parameter (line profile index), respectively. In Yb^{3+}, resonance enhancement
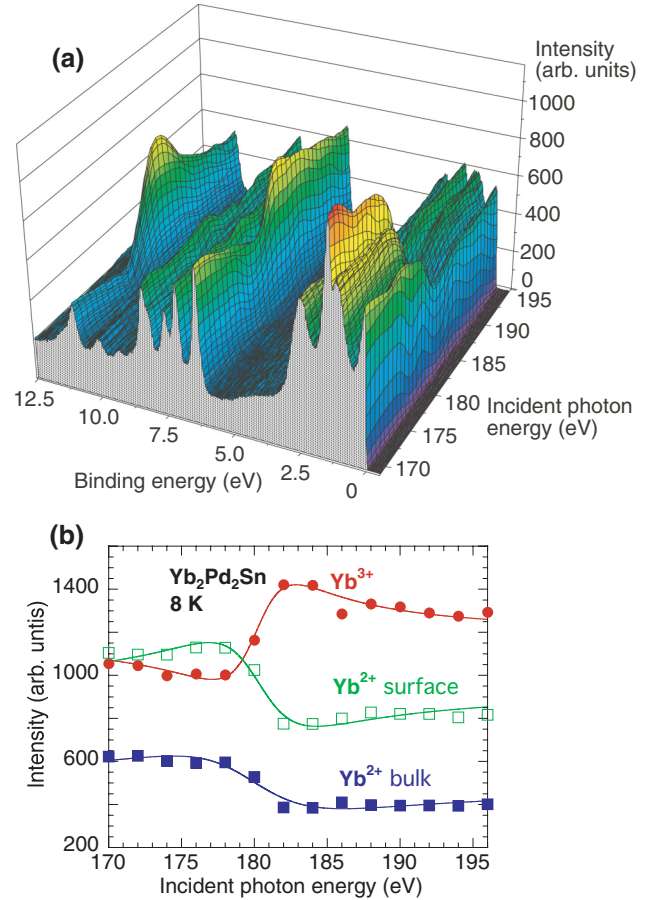

FIG. 7. (Color online) (a) Resonant photoelectron spectra of the valence band for Yb$_2$Pd$_2$Sn at 8 K in the incident energy range of $h\nu = 170$–196 eV. (b) Change in the intensity of Yb^{2+} and Yb^{3+} components derived from the fits for the resonant spectra in (a) as a function of the incident photon energies.

of the intensity occurs, whereas, in Yb^{2+}, antiresonance behavior is observed. Effective q values are estimated to be 1.092 for Yb^{3+} components and 0.912 (bulk) and 0.893 (surface) for Yb^{2+} components. To our knowledge, it is uncommon to observe both resonance and antiresonance behaviors clearly in resonant PES for a mixed valence system.[46,47] The increase in the Yb^{3+} intensity strongly correlates to the decrease in the Yb^{2+} intensity at the resonance. Yb^{2+} has a closed $4f$ shell of $4f^{14}$ so that the $4d$-$4f$ resonance does not occur directly. Furthermore, the comparison between the theoretical $4f$ partial DOS and the on- and off-resonance PES in Fig. 3(b) shows that the $4d$-$4f$ resonance strongly enhances the Yb^{3+} peaks at 11.5 eV (^3P), 11 eV (^1I), and 6 eV (^3H), whereas, the intensities for the Yb^{3+} peaks between 7 and 10 eV are only moderately affected. Further theoretical studies are needed to determine the source of this selectivity in the super-Coster-Kronig-Auger decay and its role in the resonance and antiresonance behaviors.

IV. CONCLUSION

We measured valence-band PES spectra at $h\nu = 11$ and 182 eV as a function of temperature on Yb$_2$Pd$_2$Sn and YbPd$_2$Sn. LDA + DMFT calculations of the Yb $4f$ DOS

agree well with the experimental spectra. We also measured the temperature dependence of the Yb valence using RXES. For Yb_2Pd_2Sn, our results indicate rather localized $4f$ states and a weak but finite c-f hybridization. They show that the valence of Yb is weakly fluctuating and slightly decreases with temperature, which can be explained within the SIAM. Although no anomaly was detected in the temperature dependence of the electronic structure at ambient pressure, temperature-dependent RXES measurements at high pressures are under way to address the two pressure-induced QCPs. On the other hand, the Yb valence in the superconductor $YbPd_2Sn$ is nearly $3+$ and does not depend on temperature. This indicates that the Yb $4f$ states are localized and, therefore, do not contribute to the occurrence of superconductivity. We also performed Yb $4d$-$4f$ resonant PES on Yb_2Pd_2Sn. We find that the CIS intensity variation in the Yb^{3+} and Yb^{2+} components can be fitted by a Fano profile with a resonance and an antiresonance behavior, respectively. This result points to an intimate correlation between the incident energy dependences of the Yb^{3+} and Yb^{2+} intensities. The understanding of this phenomenon will require further investigation.

*Present address: National Synchrotron Light Source II, Brookhaven National Laboratory, Upton, New York 11973.

[1] W. M. Temerman, L. Petit, A. Svane, Z. Szotek, M. Lüders, P. Strange, J. B. Straunton, I. D. Hughes, and B. L. Gyorffy, *Handbook on the Physics and Chemistry of Rare Earths*, edited by K. A. Gschneidner Jr., J.-C. G. Bünzli, and V. K. Pecharsky (North-Holland/Elsevier, Tokyo, 2009), Vol. 39, Chap. 241, p. 1.

[2] H. Yamaoka, I. Jarrige, N. Tsujii, M. Imai, J.-F. Lin, M. Matsunami, R. Eguchi, M. Arita, K. Shimada, H. Namatame, M. Taniguchi, M. Taguchi, Y. Senba, H. Ohashi, N. Hiraoka, H. Ishii, and K.-D. Tsuei, Phys. Rev. B **83**, 104525 (2011).

[3] J. M. Lawrence, P. S. Riseborough, and R. D. Parks, Rep. Prog. Phys. **44**, 1 (1981).

[4] G. R. Stewart, Rev. Mod. Phys. **73**, 797 (2001); **78**, 743 (2006).

[5] H. v. Löhneysen, A. Rosch, M. Vojta, and P. Wölfle, Rev. Mod. Phys. **79**, 1015 (2007).

[6] R. A. Gordon, Y. Ijiri, C. M. Spencer, and F. J. DiSalvo, J. Alloys Compd. **224**, 101 (1995).

[7] D. Kaczorowski, P. Rogl, and K. Hiebl, Phys. Rev. B **54**, 9891 (1996).

[8] M. Giovannini, H. Michor, E. Bauer, G. Hilscher, P. Rogl, and R. Ferro, J. Alloys Compd. **280**, 26 (1998).

[9] P. de V. du Plessis, A. M. Strydom, R. Troc, and L. Menon, J. Phys.: Condens. Matter **13**, 8375 (2001).

[10] M. Giovannini, E. Bauer, H. Michor, G. Hilscher, A. Galatanu, A. Saccone, and P. Rogl, Intermetallics **9**, 481 (2001).

[11] E. Bauer, H. Hilscher, H. Michor, C. Paul, Y. Aoki, H. Sato, D. T. Adroja, J.-G. Park, P. Bonville, C. Godart, J. Sereni, M. Giovannini, and A. Saccone, J. Phys.: Condens. Matter **17**, S999 (2005).

[12] A. Doğan, S. Rayprol, and R. Pöttgen, J. Phys.: Condens. Matter **19**, 026209 (2007).

[13] S. K. Dhar, R. Settai, Y. Ōnuki, A. Gavatanu, Y. Haga, P. Manfrinetti, and M. Pani, J. Magn. Magn. Mater. **308**, 143 (2007).

[14] M. S. Kim, M. C. Bennett, and M. C. Aronson, Phys. Rev. B **77**, 144425 (2008).

[15] E. Bauer, H. Michor, T. Muramatsu, T. Kanemasa, T. Kagayama, K. Shimizu, Y. Aoki, H. Sato, and M. Giovannini, J. Optoelectron. Adv. Mater. **10**, 1633 (2008).

[16] T. Muramatsu, T. Kanemasa, T. Kagayama, K. Shimizu, Y. Aoki, H. Sato, M. Giovannini, P. Bonville, V. Zlatic, I. Aviani, R. Khasanov, C. Rusu, A. Amato, K. Mydeen, M. Nicklas, H. Michor, and E. Bauer, Phys. Rev. B **83**, 180404(R) (2011).

[17] F. Kikuchi, K. Hara, E. Matsuoka, H. Onodera, S. Nakamura, T. Nojima, K. Katoh, and A. Ochiai, J. Phys. Soc. Jpn. **78**, 083708 (2009).

[18] E. Bauer, R. T. Khan, M. Giovannini, and C. Ritter, Phys. Status Solidi B **247**, 717 (2010).

[19] E. Bauer, G. Hilscher, H. Michor, C. Paul, Y. Aoki, H. Sato, M. Giovannini, and A. Saccone, J. Magn. Magn. Mater. **272-276**, 237 (2004).

[20] P. Giudicelli, B. Rossli, A. Stunault, J. Ollivier, A. Amato, H. Sugawara, and N. Bernhoeft, J. Magn. Magn. Mater. **272-276**, e141 (2004).

[21] P. Giudicelli and N. Bernhoeft, Europhys. Lett. **67**, 117 (2004).

[22] H. Yamaoka, I. Jarrige, N. Tsujii, J.-F. Lin, T. Ikeno, Y. Isikawa, K. Nishimura, R. Higashinaka, H. Sato, N. Hiraoka, H. Ishii, and K.-D. Tsuei, Phys. Rev. Lett. **107**, 177203 (2011).

[23] H. Yamaoka, I. Jarrige, N. Tsujii, N. Hiraoka, H. Ishii, and K.-D. Tsuei, Phys. Rev. B **80**, 035120 (2009).

[24] H. Yamaoka, I. Jarrige, N. Tsujii, J.-F. Lin, N. Hiraoka, H. Ishii, and K.-D. Tsuei, Phys. Rev. B **82**, 035111 (2010).

[25] P. Thunström, I. Di Marco, A. Gréchnev, S. Lebegue, M. I. Katsnelson, A. Svane, and O. Eriksson, Phys. Rev. B **79**, 165104 (2009).

[26] S. Lebégue, G. Santi, A. Svane, O. Bengone, M. I. Katsnelson, A. I. Lichtenstein, and O. Eriksson, Phys. Rev. B **72**, 245102 (2005).

[27] S. Lebégue, A. Svane, M. I. Katsnelson, A. I. Lichtenstein, and O. Eriksson, J. Phys.: Condens. Matter **18**, 6329 (2006).

[28] O. Grånäs, I. Di Marco, P. Thunström, L. Nordström, O. Eriksson, T. Björkman, and J. M. Wills, Comput. Mater. Sci. **55**, 295 (2012).

[29] H. Yamaoka, P. Thunström, I. Jarrige, K. Shimada, N. Tsujii, M. Arita, H. Iwasawa, H. Hayashi, J. Jiang, T. Habuchi, D. Hirayama, H. Namatame, M. Taniguchi, U. Murao, S. Hosoya, A. Tamaki, and H. Kitazawa, Phys. Rev. B **85**, 115120 (2012).

[30] K. Shimada, M. Arita, Y. Takeda, H. Fujino, K. Kobayashi, T. Narimura, H. Namatame, and M. Taniguchi, Surf. Rev. Lett. **9**, 529 (2002).

[31] M. Arita, K. Shimada, Y. Takeda, M. Nakatake, H. Namatame, and M. Taniguchi, Surf. Rev. Lett. **9**, 535 (2002).

[32] A. Georges, G. Kotliar, W. Krauth, and M. J. Rozenberg, Rev. Mod. Phys. **68**, 13 (1996).

[33] G. Kotliar, S. Y. Savrasov, K. Haule, V. S. Oudovenko, O. Parcollet, and C. A. Marianetti, Rev. Mod. Phys. **78**, 865 (2006).

[34] J. M. Wills, M. Alouani, P. Andersson, A. Delin, O. Eriksson, and O. Grechnyev, *Full-Potential Electronic Structure Method, Electronic Structure and Physical Properties of Solids*, Springer Series in Solid-State Sciences (Springer-Verlag, Berlin, 2010).

[35] A. Grechnev, I. Di Marco, M. I. Katsnelson, A. I. Lichtenstein, J. Wills, and O. Eriksson, Phys. Rev. B **76**, 035107 (2007).

[36] I. Di Marco, J. Minár, S. Chadov, M. I. Katsnelson, H. Ebert, and A. I. Lichtenstein, Phys. Rev. B **79**, 115111 (2009).

[37] J. Hubbard, Proc. R. Soc. London, Ser. A **276**, 238 (1963).

[38] A. I. Lichtenstein and M. I. Katsnelson, Phys. Rev. B **57**, 6884 (1998).

[39] V. T. Rajan, Phys. Rev. Lett. **51**, 308 (1983).

[40] M. P. Seah and W. A. Dench, Surf. Interface Anal. **1**, 2 (1979).

[41] J. J. Yeh and I. Lindau, At. Data Nucl. Data Tables **32**, 1 (1985).

[42] K. Kummer, Y. Kucherenko, S. Danzenbächer, C. Krellner, C. Geibel, M. G. Holder, L. V. Bekenov, T. Muro, Y. Kato, T. Kinoshita, S. Huotari, L. Simonelli, S. L. Molodtsov, C. Laubschat, and D. V. Vyalikh, Phys. Rev. B **84**, 245114 (2011).

[43] H. Yamaoka, I. Jarrige, N. Tsujii, A. Kotani, J.-F. Lin, F. Honda, R. Settai, Y. Ōnuki, N. Hiraoka, H. Ishii, and K.-D. Tsuei, J. Phys. Soc. Jpn. **80**, 124701 (2011).

[44] M. Aldén, B. Johansson, and H. L. Skriver, Phys. Rev. B **51**, 5386 (1995).

[45] H. Yamaoka, M. Matsunami, R. Eguchi, Y. Ishida, N. Tsujii, Y. Takahashi, Y. Senba, H. Ohashi, and S. Shin, Phys. Rev. B **78**, 045125 (2008).

[46] S. W. Han, J.-S. Kang, K. H. Kim, J. D. Lee, J. H. Kim, S. C. Wi, C. Mitra, P. Raychaudhuri, S. Wirth, K. J. Kim, B. S. Kim, J. I. Jeong, S. K. Kwon, and B. I. Min, Phys. Rev. B **69**, 104406 (2004).

[47] W. R. Flavell, A. G. Thomas, D. Tsoutsou, A. K. Mallick, M. North, E. A. Seddon, C. Cacho, A. E. R. Malins, S. Patel, R. L. Stockbauer, R. L. Kurtz, P. T. Sprunger, S. N. Barilo, S. V. Shiryaev, and G. L. Bychkov, Phys. Rev. B **70**, 224427 (2004).